Mean-field approach to ferromagnetism in (III,Mn)V diluted magnetic semiconductors at low carrier densities

Mona Berciu[1,2] and R. N. Bhatt[2]

[1]*Department of Physics and Astronomy, University of British Columbia, Vancouver British Columbia Canada V6T 1Z1*
[2]*Department of Electrical Engineering, Princeton University, Princeton, New Jersey 08544, USA*

We present a detailed study, within the mean-field approximation, of an impurity band model for III-V diluted magnetic semiconductors. Such a model should be relevant at low carrier densities, below and near the metal-insulator transition. Positional disorder of the magnetic impurities inside the host semiconductor is shown to have observable consequences for the shape of the magnetization curve. Below the critical temperature the magnetization is spatially inhomogeneous, leading to very unusual temperature and magnetic field dependence of the average magnetization as well as specific heat. A metal-insulator transition is also observed, with a mobility edge inside the impurity band, in agreement with experimental measurements.

I. INTRODUCTION

Diluted magnetic semiconductors (DMS) are semiconductors of the general type $A_{1-x}M_xB$, where AB is either a II-VI or a III-V semiconductor and M a magnetic element, most commonly Mn. Substitution of a small fraction x of the element A by Mn impurities (and in the case of II-VI semiconductors an additional charge dopant, such as P on the B site) leads to the emergence of a semiconductor with ferromagnetic properties.[1] This is due to the interactions of the $S = \frac{5}{2}$ Mn spins (coming from the half-filled 3d shell of the Mn) with the spins of the charge carriers introduced by the Mn dopants, or by the additional dopant, for II-VI semiconductors. This opens up the possibility to manipulate (through doping) not only the transport, but also the magnetic properties of the semiconductor and thus, the potential to develop "spintronic" devices which combine storage (memory) functionalities with information processing functionalities.

The recent demonstration of Curie temperatures of up to 150 K in $Ga_{1-x}Mn_xAs$ samples with $x \approx 0.05$, grown at low temperatures using molecular-beam epitaxy (MBE) techniques,[2–6] has heightened the interest in understanding the physics of these alloys. By now, it is well established that the main magnetic interaction is an antiferromagnetic (AFM) exchange between the Mn spins and the charge-carrier spins. As a result, an effective ferromagnetic (FM) interaction arises between the Mn spins through carrier-induced ferromagnetism. Several theories, most notably Ruderman-Kittel-Kasuya-Yosida (RKKY),[7] have been used to explain, within a mean-field approximation, this phenomenon. More recently, dynamic correlations as well as arbitrary itinerant-carrier spin polarizations have been included.[8] All these models assume that as a result of screening by charge carriers, Coulomb interactions become negligibly small and the charge carriers (the holes) occupy a Fermi sea in the valence band. This leads to a spatially homogeneous distribution of the holes throughout the entire system and therefore results in a homogeneous magnetization, in which disorder in Mn positions (always present in such alloys) plays little or no role.

However, Mn impurities in a III-V semiconductor create a trapping potential for holes.[9] The associated acceptor levels are about 100 meV above the top of the valence band, for GaAs, and interactions will lead to their splitting into an impurity band.[10,11] At $T=0$, the holes occupy the states of lowest energy and therefore they first fill the states in the impurity band. Only if the Fermi energy (or thermal energy k_BT) is large enough are states in the valence band occupied as well. It has been found experimentally that these alloys are heavily compensated, leading to rather small hole concentrations, of the order of 10–30 % of the Mn concentration.[12] The corresponding small Fermi energy implies a long screening length for the Coulomb interactions, and opens up the possibility that holes are actually moving (through hopping processes) in the impurity band formed of states localized about the Mn impurities. As a result, randomness in the position of the Mn spins could be expected to play an important role in defining the properties of these compounds.

There is strong experimental support for this scenario. Low-temperature dc conductivity is consistent with Mott variable-range hopping behavior.[4,13] Photoemission spectroscopy has revealed the existence of the impurity band in $Ga_{1-x}Mn_xAs$ with $x=0.035$ (very close to the metal-insulator transition),[14] while scanning tunneling microscope study[15] demonstrates the existence of an impurity band in (Ga,Mn)As samples with $x=0.005$. More recently, a detailed photoemission study[16] for Mn concentrations $x=1–6$ % finds that the Fermi level is always above the top of valence band of the undoped GaAs compound, clearly indicating the existence of states inside the gap. Finally, recent optical spectroscopy studies[17] show the existence of features in the optical conductivity consistent with the existence of an impurity band for $x=0.0001$ and $x=0.05$ samples.

In this paper we investigate, at the mean-field level, a simple model in which holes move in a band formed of impurity states, completely neglecting the higher-energy valence-band states. Since we find typical Fermi energies of a few tens of millielectron volt, smaller than the $\sim 100–200$ meV between the impurity band and the valence

band, this seems to be a reasonable first-order approximation. This model allows us to understand in a rather simple frame a number of nontrivial effects of the disorder in Mn positions on the magnetic and transport properties of these compounds (some of which have already been reported in Ref. 18). In particular, we find a spatially inhomogeneous magnetization, very unlike the homogeneous magnetization predicted by models with holes occupying a Fermi sea in the valence band. However, our results show some qualitative agreement (such as very wide distributions of effective couplings, due to disorder) with more recent work[19] on such ''metallic'' models, which also include unscreened Coulomb interactions between the holes and Mn centers and as a result are sensitive to disorder in Mn positions. This is encouraging, as it suggests some convergence of the phenomenology predicted by the higher density (metallic) models and the low-density (insulating) models. Clearly, a full quantitative understanding of these compounds will necessitate a detailed modeling of the impurity band and inclusion of the valence-band states with proper description of other factors such as screening (on a proper, local scale, taking into account strong charge inhomogeneities) as well as various defects responsible for compensation.

The paper is organized as follows. In Sec. II we describe the model Hamiltonian, the self-consistent mean-field approximation as well as the specific parameters used in the numerical calculations. It is important to emphasize that although we chose numbers from the literature specific to the GaMnAs problem for illustration purposes, similar arguments and physics would hold for other III-V compounds. In Sec. III we present our results. We first analyze the hypothetical case in which all Mn impurities are ordered in a simple cubic lattice. This allows us to understand the unusual shape of the magnetization curves we obtain. More importantly, it allows us to clearly identify the nontrivial effects of randomness (disorder) in the Mn positions. These are analyzed in some detail and a clear physical picture of their importance to the problem emerges. We also analyze the metal-insulator transition, the effects of on-site random disorder, as well as other possible interactions. The sensitivity of our results to variations in the impurity band parameters is also discussed. Finally, Sec. IV contains a summary and conclusions.

II. MODEL

We assume that Mn only substitutes for the group III element of the III–V semiconductor with zinc-blende structure [the effects of interstitial Mn (Ref. 20) is neglected throughout this work]. $\vec{R}_i, i=1,\ldots,N_d$ are the random positions of the N_d Mn dopants. Each Mn impurity is associated with a spin-$\frac{5}{2}$ from its half-filled $3d$ shell. The valence-II Mn is an acceptor and it can trap a hole in a shallow level, characterized by a Bohr radius a_B. Let N_h be the total number of holes trapped about various Mn sites, and $p=N_h/N_d$ the relative hole concentration.

Although the charge carriers are holes, in the following we use an ''electron'' formalism: we analyze an equivalent system doped with hypothetical donors, with impurity levels

below a conductionlike band. The main difference between the two models is (i) the hole spin is $\frac{3}{2}$ and (ii) the envelope wave function of hole has cubic symmetry, rather than spherical symmetry of a donor. This leads to some quantitative differences (as has been shown by MacDonald and co-workers for free holes in Ref. 21) but the essential aspects of the problem, namely, (a) disorder and (b) the effect of impurity potentials, which we concentrate on here, remain substantially unaffected.

The Hamiltonian we study is

$$
\begin{aligned}
\mathcal{H}=&\sum_{i,j} t_{ij}c_{i\sigma}^{\dagger}c_{j\sigma}+\sum_{i} u(i)c_{i\sigma}^{\dagger}c_{i\sigma}+\sum_{i,j} J_{ij}\vec{S}(i)\\
&\times\left(c_{j\alpha}^{\dagger}\frac{1}{2}\vec{\sigma}_{\alpha\beta}c_{j\beta}\right)-g\mu_B H\sum_{i} \frac{\sigma}{2}c_{i\sigma}^{\dagger}c_{i\sigma}\\
&-\widetilde{g}\mu_B H\sum_{i} S^z(i).
\end{aligned}
\tag{1}
$$

Here, $c_{i\sigma}^{\dagger}$ is the creation operator of a charge carrier with spin σ in the bound orbital associated with the ith Mn impurity. The first term describes charge carriers hopping between Mn sites, with a hopping t_{ij} dependent on the distance $r=|\vec{R}_i-\vec{R}_j|$. We use an exponential form like for hydrogenic orbitals[22] $t(r)=2(1+r/a_B)\exp(-r/a_B)$ Ry (see Appendix for a justification). We present detailed results for this case; however in Sec. III F we discuss the changes that result for other hopping models. From these different cases we discern the universal aspects of the impurity models. The Rydberg (Ry) equals the binding energy of the charge carrier to the shallow trap E_b. The heavily compensated nature of the system gives rise to random potentials coming from the charged centers responsible for compensation. We model this through an on-site random potential $u(i)$ which leads to the second term in Eq. (1). Complete modeling would require a self-consistent determination of this potential taking in consideration screening processes. The third term describes the AFM interaction between Mn spins $\vec{S}(i)$ and charge-carrier spins. Since the Mn spins are very localized (the $3d$ shell has a radius of the order 1–2 Å) the AFM exchange integral is taken to be of the form $J_{ij}=J|\phi(i,j)|^2=J\exp(-2|\vec{R}_i-\vec{R}_j|/a_B)$, reflecting the probability of finding the charge carrier in the s-type shallow level about impurity j near the ith Mn spin. In this notation, J is simply the AFM exchange integral of an isolated localized hole centered at a Mn impurity with the spin of the Mn. The last two terms describe interactions with an external magnetic field H.

A. Mean-field approximation

We treat the AFM interaction at the mean-field level, described by the factorization[23]

$$
\vec{S}(i)\cdot\hat{\vec{\sigma}}_j\to S_{\text{Mn}}(i)\hat{\sigma}_j^z+S^z(i)s_h(j)-S_{\text{Mn}}(i)s_h(j),
\tag{2}
$$

where $S_{\text{Mn}}(i)=\langle S^z(i)\rangle$ and $s_h(j)=\langle\hat{\sigma}_j^z\rangle$ are the expectation values of the ith Mn spin and of the total spin created by

charge carriers at the jth Mn site, respectively, and must be computed self-consistently. For simplicity of notation, we used $\hat{\vec{\sigma}}_j = c^{\dagger}_{j\alpha} \frac{1}{2} \vec{\sigma}_{\alpha\beta} c_{j\beta}$ in Eq. (2).

The mean-field Hamiltonian has three parts

$$\mathcal{H}_{MF} = \mathcal{H}_{spin} + \mathcal{H}_{cc} + \mathcal{H}_{const}. \tag{3}$$

The spin Hamiltonian is $\mathcal{H}_{spin} = -\Sigma_i H_i S^z(i)$, where

$$H_i = \tilde{g}\mu_B H - J\sum_j |\phi(i,j)|^2 s_h(j) \tag{4}$$

is the effective magnetic field for the Mn spin at site i. The expectation value for the Mn spins is

$$S_{Mn}(i) = \mathcal{B}_S(\beta H_i), \tag{5}$$

where $\mathcal{B}_S(x) = (S + \frac{1}{2})\coth[(S + \frac{1}{2})x] - \frac{1}{2}\coth x/2$ is the Brillouin function for spin $S = 5/2$ and $\beta = 1/k_B T$.

The charge carrier Hamiltonian can be rewritten as

$$\mathcal{H}_{cc} = \sum_{i,j} t_{ij} c^{\dagger}_{i\sigma} c_{j\sigma} + \sum_{i\sigma} (\epsilon_{i\sigma} - \mu) c^{\dagger}_{i\sigma} c_{i\sigma}, \tag{6}$$

where

$$\epsilon_{i\sigma} = \frac{\sigma}{2}\left(J\sum_j \left| \phi(i,j) \right|^2 S_{Mn}(j) - g\mu_B H \right) + u(i) \tag{7}$$

is the effective on-site energy. A chemical potential μ is added to treat the carriers in grand-canonical ensemble.

The charge-carrier Hamiltonian can be diagonalized $\mathcal{H}_{cc} = \Sigma_{n\sigma}(E_{n\sigma} - \mu)a^{\dagger}_{n\sigma}a_{n\sigma}$, using the unitary transformation $a^{\dagger}_{n\sigma} = \Sigma_i \psi_{n\sigma}(i) c^{\dagger}_{i\sigma}$. Here $\psi_{n\sigma}(i)$ is the amplitude of probability to find a charge carrier occupying level n with spin σ to be at site i. μ is given by

$$N_h = \sum_{n\sigma} f(E_{n\sigma}), \tag{8}$$

where $f(E_{n\sigma}) = \{\exp[\beta(E_{n\sigma} - \mu)] + 1\}^{-1}$ is the Fermi occupation probability of the level $(n\sigma)$. Then, the average spin created by charge carriers at site i is

$$s_h(i) = \sum_{n,\sigma} \frac{\sigma}{2}|\psi_{n\sigma}(i)|^2 f(E_{n\sigma}). \tag{9}$$

Finally, $\mathcal{H}_{const} = -J\Sigma_{i,j}|\phi(i,j)|^2 S_{Mn}(i)s_h(j)$ contains the constant terms from the mean-field factorization.

The internal energy is $U = \langle \mathcal{H}_{MF} \rangle = -\tilde{g}\mu_B H\Sigma_i S_{Mn}(i) + \Sigma_{n\sigma}E_{n\sigma}f(E_{n\sigma})$, while the specific heat of the system is $C_V(T) = \partial U(T)/\partial T$. Other quantities of interest can also be computed.

We solve the mean-field equations (4)–(9) using an iterative algorithm. We start with a guess for the initial configuration $S_{Mn}(i)$ for each temperature T of interest (details about this are provided in Sec. III B). We numerically diagonalize the charge-carrier Hamiltonian (6) and find the charge-carrier eigenvalues, eigenfunctions, as well as the chemical potential from Eq. (8). We then compute $s_h(j)$ [Eq. (9)] and H_i [Eq. (4)]. The new values for $S_{Mn}(i)$ are then obtained from Eq.

(5) and the iterations are repeated until self-consistency is achieved. We define self-consistency as corresponding to the situation where the largest absolute variation of the on-site charge-carrier energies $\epsilon_{i\sigma}$ [Eq. (7)] between two successive iterations is less than 10^{-3} meV. This corresponds to relative errors of 10^{-5} or less for all computed quantities.

B. Parameters

We consider a $N \times N \times N$ fcc sublattice of the valence-III element, of lattice constant a ($a = 5.65$ Å for GaAs), with periodic boundary conditions. The Mn doping is characterized by $x = N_d/4N^3$, leading to a Mn concentration $c_{Mn} = 4x/a^3$. The hole concentration is $c_h = pc_{Mn}$, where $p = N_h/N_d$. Values of interest are $x = 0.01–0.05$ and $p = 10–30\%$.[1,12] The choice of the system size N is described in the following section.

The parameters we use are specific to $Ga_{1-x}Mn_xAs$. The binding energy is $E_b = 112.4$ meV $= 1$ Ry.[9] Using the Luttinger Hamiltonian in the spherical approximation we find the effective mass for the heavy hole to be $m_h = m_e/[\gamma_1 - (6\gamma_3 + 4\gamma_2)/5] = 0.56 m_e$, where the γ coefficients for GaAs are $\gamma_1 = 7.65$, $\gamma_2 = 2.41$, and $\gamma_3 = 3.28$.[9] This gives an estimate of the Bohr radius as[10] $a_B = \hbar/\sqrt{2m_h E_b} = 7.8$ Å. This is in excellent agreement with another estimate, obtained by assuming that the hole is bound to its impurity by a pure Coulomb attraction, in which case $E_b = e^2/(2\epsilon a_B)$. Using the value $\epsilon = 10.66$ for GaAs leads to $a_B = 7.82$ Å. While this agreement is probably fortuitous, similar values have been used in literature.[4] Besides the Rydberg, a second energy scale is provided by the exchange integral. We set $J = 3\epsilon = 15$ meV, where $\epsilon = 5$ meV is the value obtained in Ref. 9 for the AFM interaction of an isolated hole with the spin of its own trapping Mn impurity. A factor of 3 is the simplest way to account for the fact that the heavy holes have spin projections $j_z = \pm\frac{3}{2}$, while in our model they are modeled as $s_z = \pm\frac{1}{2}$ objects. The final parameter W characterizes the on-site disorder due to uncompensated impurities. We assume that $u(i)$ has a uniform distribution in a range $[-W, W]$. Following Ref. 10 we estimate $W \approx e^2/\epsilon\tilde{r}$, where $\tilde{r} \sim 1/n_{Mn}^3$ is roughly the average distance between Mn impurities. For the typical charge carrier concentration considered $c_h = 1.5 \times 10^{20}$ cm^{-3} and $p = 10\%$, we find $\tilde{r} \sim 9$ Å $\sim a_B$, which suggests $W \sim 1$ Ry. To conclude, in the absence of external magnetic fields the problem has five dimensionless parameters: J/E_b, a_B/a, $n_h a_B^3$, x, and W/E_b.

III. RESULTS

A. Simple cubic superlattice of Mn

We first consider the simplified case of Mn impurities placed in an ordered cubic structure, with a superlattice constant $a_L = a/(4x)^{1/3}$. While only concentrations x for which a_L is commensurate with a would be physically acceptable, we disregard the underlying GaAs lattice in this particular case. We also set the on-site disorder $u(i) = 0$, and turn off the external magnetic field.
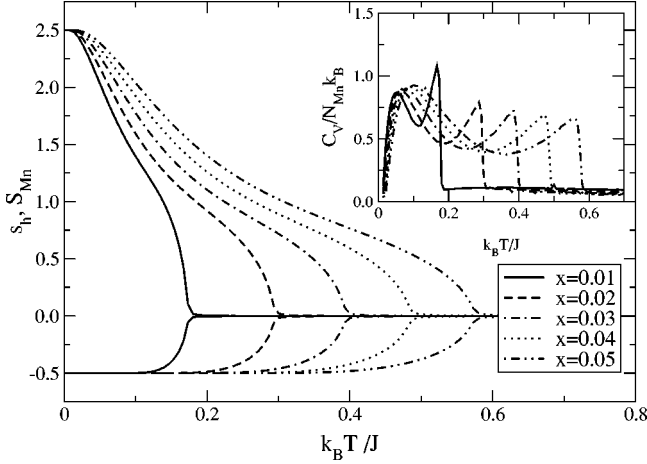
FIG. 1. The average Mn spin S_{Mn} and the average spin per charge-carrier $s_h = \Sigma_i s_h(i)/N_h = s_{hole}/p$ for doping concentrations $x = 0.01 - 0.05$ and $p = 10\%$. The Mn spin curves have an unusual shape (see text). The inset shows the specific heat per Mn as a function of temperature. The lower peak is due to Mn spin fluctuations, while the upper peak is due to charge-carrier fluctuations.

FIG. 2. The average Mn spin S_{Mn} and the average spin per charge-carrier s_h for $p = 5, 10, 25,$ and 40%. The Mn concentration is fixed at $x = 0.02$. For large p, S_{Mn} regains the shape expected for conventional ferromagnets.

For the ordered case, translational symmetry implies $s_h(i) = s_{hole}, S_{Mn}(i) = S_{Mn}$ for all sites i of the cubic Mn superlattice. As a result, $\mathcal{H}_{cc}$ is diagonalized with plane waves, and Eqs. (4)–(9) reduce to $S_{Mn} = -\mathcal{B}(\beta J_{eff} s_{hole})$ and $s_{hole} = (1/16\pi^3) \int d\vec{k} \Sigma_\sigma \sigma f(E_{\vec{k}\sigma})$. The chemical potential is given by $p = (1/8\pi^3) \int d\vec{k} \Sigma_\sigma f(E_{\vec{k}\sigma})$ and the charge-carrier eigenenergies are $E_{\vec{k}\sigma} = \epsilon(\vec{k}) + (\sigma/2) J_{eff} S_{Mn}$. Here, $\vec{k}$ is measured in units of $1/a_L$, and the integrals are performed over the first Brillouin zone $-\pi < k_\alpha \le \pi, \quad \alpha = x, y, z$. Also, $\epsilon(\vec{k}) = \Sigma_{i \ne 0} t(r_i) e^{i\vec{r}_i \cdot \vec{k}}$ and $J_{eff} = J\Sigma_i |\phi(i)|^2 = J\Sigma_i e^{-2r_i/a_B}$, where the sums are performed over the whole crystal.

The self-consistent values of $0 < S_{Mn} < 5/2$ and the average charge-carrier spin $-1/2 < s_h = \Sigma_i s_h(i)/N_h = s_{hole} N_d/N_h < 0$ obtained for $x = 0.01 - 0.05$ and $p = 10\%$ are shown in Fig. 1. The overall signs reflect the AFM alignment of the charge-carrier and Mn spins. The total magnetization of the sample, obtained by adding the Mn and charge-carrier contributions, is similar to the S_{Mn} curve, since the number of Mn spins is $1/p \sim 3-10$ times larger than the number of charge-carrier spins. The magnetization curves do not have the typical shape of conventional ferromagnets. In fact, each curve shows three different regimes. Just below T_c there is a region where neither the charge carriers nor the Mn spins are yet fully polarized. The gap $J_{eff} S_{Mn}$ between the $\sigma = \downarrow$ and $\sigma = \uparrow$ charge-carrier bands increases quickly as the T decreases. Since there are fewer charge carriers, they are the first to fully polarize to $s_{hole} = p s_h = -0.5p$. For lower T, the Mn spins are in a constant effective magnetic field $H = J_{eff} s_{hole} = -0.5p J_{eff}$. If $\beta H \ll 1$, the Brillouin function may be linearized and $S_{Mn} \sim J_{eff}/k_B T$ (the Curie law). This explains the uncharacteristic concave upward shape of the Mn spin magnetization in this intermediate temperature regime. Finally, for very low temperatures, the Mn spins also become fully polarized.
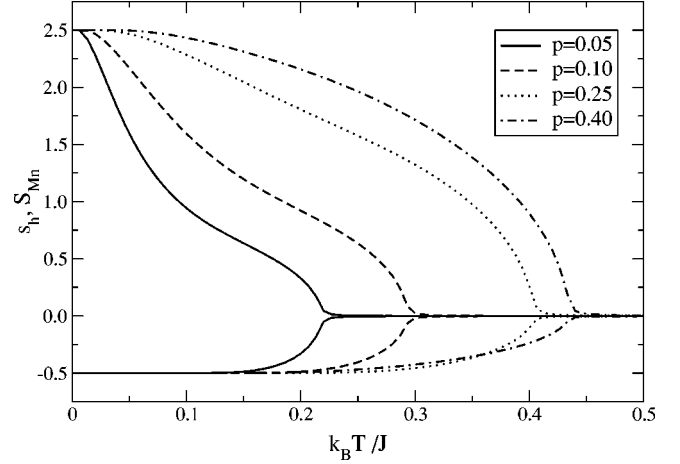
The inset of Fig. 1 shows the specific heat per Mn impurity for the same parameters. In all cases we see two distinct contributions. At low T, the charge carriers are all "frozen" at the bottom of the $\sigma = \downarrow$ band, and all the entropy is due to fluctuations in the Mn spins. This can be easily checked by computing $C_V^{spins} = dU_{spin}/dT$, with $s_{hole} = -0.5p$ and $U_{spin} = \langle \mathcal{H}_{spin} \rangle$, which recaptures the entire lower peak. At higher T values the Mn spins are almost free (the effective magnetic field polarizing them is very small), and near T_c the entropy is dominated by spin fluctuations of the charge carriers.

As the relative concentration p increases, one expects that T below which charge carriers become fully polarized decreases (since E_F is large) and the unusual intermediary regime where $S_{Mn} \sim 1/k_B T$ is restricted to smaller ranges. As a result, the magnetization curves should regain the characteristic shape of conventional FM. This is confirmed in Fig. 2, where the average charge-carrier and Mn spins are plotted for $p = 5, 10, 25,$ and 40%.

It is interesting to note that the T_c values obtained for this homogeneous case using the nominal parameters from literature are actually in good agreement with experimentally measured values. In Fig. 3 we plot T_c for three GaMnAs samples,[12] which are estimated to have $p = 5-10\%$, in agreement with our estimates. However, as we show in the following, disorder has a large effect on T_c. At the same time, the mean-field approximation itself underestimates thermal fluctuations, and therefore substantially overestimates T_c.[24] We conclude that the good agreement shown in Fig. 3 is likely fortuitous, but it should be taken as an indication that this simple model gives the right order of magnitude of T_c.

B. Effects of disorder in Mn positions

We now analyze the effects of randomness in the positions of the Mn on the shape of the magnetization and the value of T_c. We continue to assume no on-site disorder po-
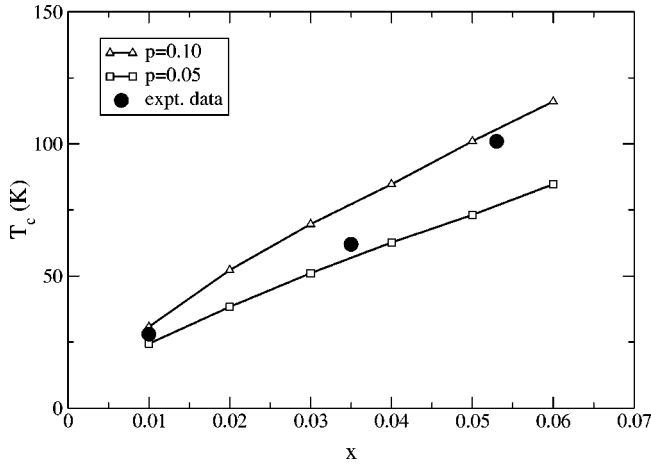
FIG. 3. Comparison between experimental values of T_c (full circles, from Ref. 10), and mean-field values for the ordered case. The good agreement indicates that the parameters used here are reasonable.

FIG. 4. The average Mn and carrier spins S_{Mn} and s_h for $x = 0.00926$ and $p = 10\%$. In increasing order of T_c, the curves are for ordered, weakly disordered, moderately disordered, and completely random distributions of Mn (see text).

tential $[u(i)=0]$ and zero external magnetic field. Due to positional disorder, the system is no longer homogeneous and we have to consider finite-size lattices. We choose randomly the positions of the N_d Mn spins and solve numerically Eqs. (4)–(9) self-consistently for each site. The linear size N of the lattice is chosen so as to minimize finite-size effects. These are monitored through their effect on the magnetization curves (especially on T_c) and the total density of states (DOS). Finite-size effects become negligible for $N_h \sim 50$. Sizes studied vary from $N=14$, $N_d=548$, $N_h=55$ for $x=0.05$, to $N=24$, $N_d=512$, $N_h=51$ for $x=0.00926$.

Equations (4)–(9) generally admit several self-consistent solutions, depending on the initial values used in the first iteration. For *biased* initial values, we start the first iteration at the lowest T value of interest assuming all Mn spins fully polarized, $S_{Mn}(i)=5/2$; at higher T, we use as initial values the self-consistent results found at the previous (lower) T studied. This insures that we find the self-consistent solutions with the largest possible magnetization. For *random* initial values both the magnitude and the sign of $S_{Mn}(i)$ are chosen randomly for each site for all T considered. The total magnetizations obtained in this case are smaller or equal to the maximum possible value (obtained for biased initial values), due to the appearance of regions with local magnetizations pointing in different directions. We investigated over 150 samples of varying sizes $N=14–24$ corresponding to $x = 0.009\,26–0.05$ and $p = 10–30\,\%$. In all cases, the most polarized (biased) state has been found to have the lowest total free energy in our model. For larger x, we find that most random initial samples always converge to the biased limit, signifying a more robust magnetization than at lower x. We conclude that for this range of parameters the system is FM, and the biased configurations give the most stable mean-field configurations.

The effects of positional disorder of the Mn on the magnetization curves are summarized in Fig. 4, which plots the average Mn and charge-carrier spins as a function of temperature, for four different distributions of Mn spins. All correspond t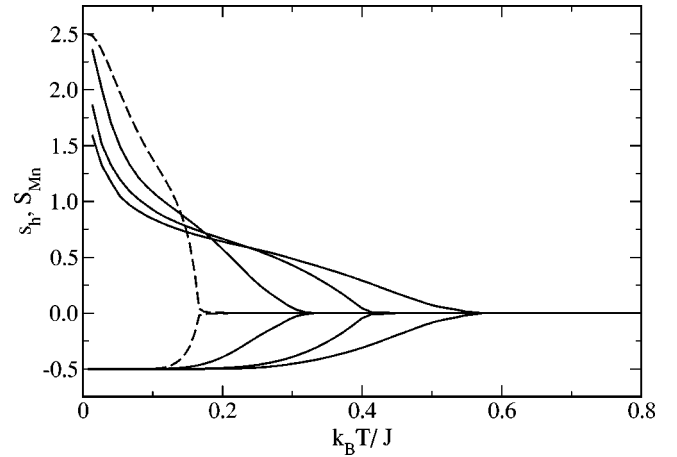o $x=0.009\,26$ and $p=10\%$. The curve with the lowest T_c is for an ordered Mn superlattice, with $a_L = 3a$. The next curve corresponds to a weak disorder configuration, in which each Mn is allowed to randomly move to one of the 12 nearest neighbors of the underlying fcc sublattice. The third curve corresponds to a medium disorder configuration in which Mn impurities are allowed to pick any sites on the fcc sublattice, as long as the distance between any two of them is at least $2a$. Finally, the curve with the highest T_c corresponds to a completely random (strong disorder) Mn configuration. Figure 4 shows that the shape of the magnetization curves is significantly changed by positional disorder. T_c is increased, while the curves become more concave, with Mn spins not reaching the saturation limit $S_{Mn} = 5/2$ until very low T. While this increase of T_c with disorder may seem counterintuitive, it has a physical explanation. In the disordered sample there are regions of higher local concentration of Mn, where the charge-carrier wave functions are peaked. Thus, the effective interactions between holes and the Mn spins in these regions are enhanced, leading to an increase of T_c. On the other hand, Mn spins in the regions devoid of holes are only very weakly interacting with holes, and therefore do not order magnetically unless temperatures are extremely small.

This point can be illustrated by looking at a histogram of the total density of charge carriers at site i, defined as

$$\rho(i) = \sum_j |\phi(i,j)|^2 \langle c_{j\uparrow}^\dagger c_{j\uparrow} + c_{j\downarrow}^\dagger c_{j\downarrow} \rangle. \qquad (10)$$

Since at low temperatures only spin-down charge-carrier states are significantly occupied, we can also interpret $\rho(i)$ as being proportional to the effective magnetic field acting on the ith Mn spins [see Eq. (4) for $H=0$]. In Fig. 5(a) we show, on a logarithmic plot, such a histogram obtained for 25 random Mn configurations with $x=0.009\,26$ and $p=10\%$ at $k_B T/J = 0.000\,6$ (dotted line) and $k_B T/J = 0.6$ (full line). The vertical line marks the value $\rho = p\Sigma_i \exp(-2r_i/a_B)$ for an ordered Mn superlattice. For small concentrations x the sum is roughly equal to unity, and the charge-carrier density and

FIG. 6. Magnetizations for 25 realizations of Mn positional disorder for $x=0.05$. The elongated tails near T_c are due to polarization of a few very dense clusters of Mn, and should be disordered by thermal fluctuations.
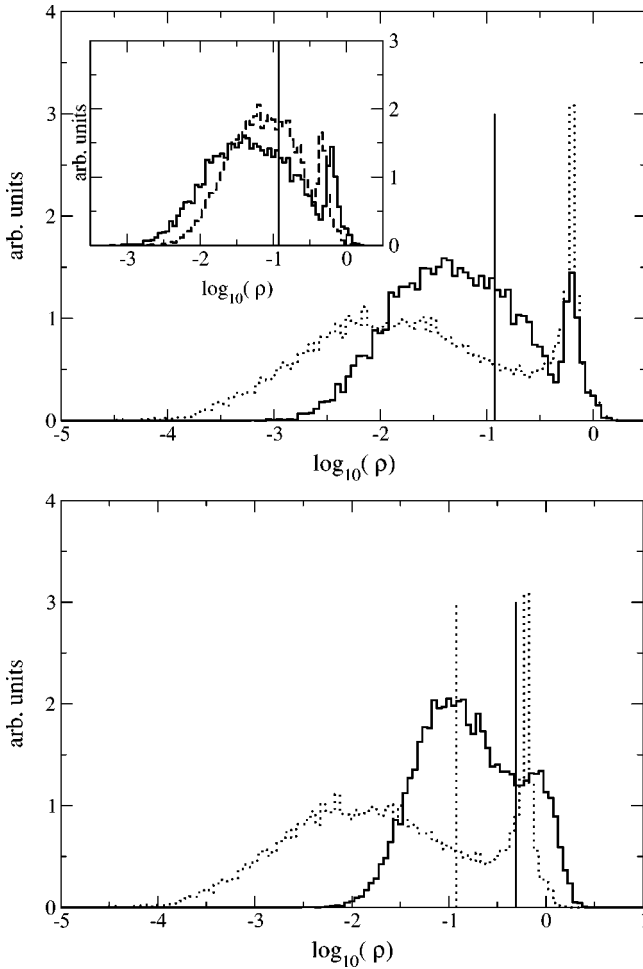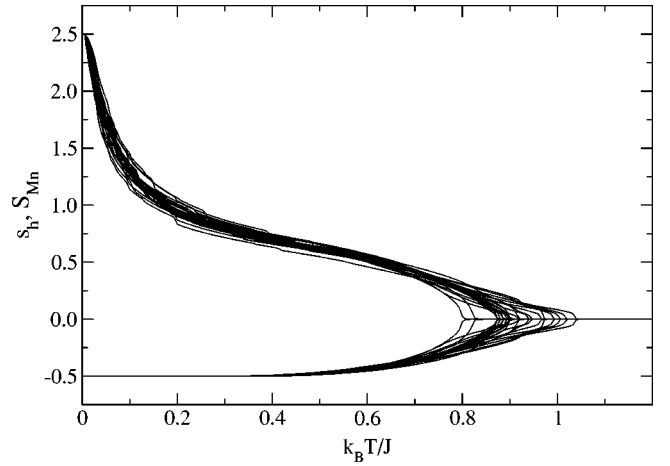
FIG. 5. (a) Histogram of $\log_{10}\rho(i)$ [Eq. (10)] for random Mn configuration with $x=0.009\,26$ and $p=10\%$. Dotted (full) lines correspond to $k_BT/J=0.000\,6$, $(k_BT/J=0.6)$. The vertical line marks the value of ρ for an ordered Mn lattice. Inset: Same for $k_BT/J=0.6$ (full line) and $k_BT/J=1.5$ (dotted line). (b) Comparison between the histograms for $x=0.009\,26$ (dotted line) and $x=0.05$ (full line). Both systems have $p=10\%$ and $k_BT/J=0.000\,5$. Vertical lines show the corresponding values for the ordered systems.

effective magnetic field at each Mn site is p and Jp, respectively. For the random (disordered) configurations, a double-peaked structure is clearly visible. One peak is centered at ≈ 0.6, well above the ordered value for ρ, and a second much broader peak centered at exponentially small values $\approx 10^{-2} \ll p$. The large values show that some Mn sites have large local charge-carrier densities, which strongly polarize the respective Mn spins up to high T, defining a T_c much higher than that of the homogeneous system. The rest of the Mn sites have small charge-carrier densities $\rho(i)$ and very quickly become depolarized with increasing T, leading to the fast decrease of S_{Mn} at low-T values. This phenomenology has been recaptured accurately by dividing the spins into strongly vs weakly interacting, depending on whether their effective magnetic field is larger or smaller than the corresponding thermal energy.[25] A mix of ferromagnetic/paramagnetic contributions to the $M(H)$ curves, which can be attributed to strongly/weakly interacting spins, has also

been observed experimentally.[26] As T increases to $k_BT/J=0.6$ (just below T_c for these parameters) and $k_BT/J=1.5 \gg k_BT_c/J$ [inset of Fig. 5(a)], the double-peaked structure is still apparent, although narrowed and with lower weight in the higher peak. This shows that as T is lowered below T_c, the charge-carrier wave functions become more concentrated inside the most dense clusters of Mn, where supplementary magnetic exchange energy can be gained. This increases the weight of the higher $\rho(i)$ peak, whereas further depopulation of the rest of the sample pushes the low edge of the distribution towards lower values. These variations occur close to T_c; for $k_BT/J<0.3$ the distribution is already converged to its low-T shape.

In Fig. 5(b) we compare the low-T histograms for $x=0.009\,26$ (dotted) and $x=0.05$ (full lines). The vertical lines again show the corresponding values for the homogeneous (ordered) systems. For $x=0.05$ the double-peaked structure is also clearly visible, but the whole histogram shifts to higher $\rho(i)$ values. This is consistent with overall increased interactions for larger charge-carrier concentrations. [It is worth pointing that for $x=0.05$ there are sites where $\rho(i)>1$ ($\log_{10}[\rho(i)]>0$). Since the probability of finding a hole at any site $p(i)=\langle c_{i\uparrow}^\dagger c_{i\uparrow}+c_{i\downarrow}^\dagger c_{i\downarrow}\rangle<1$, this suggests that some Mn spins strongly interact with several nearby charge carriers [see Eq. (10)]. For $x=0.009\,26$, however, $\rho(i)<1$ for all sites, showing that Mn spins interact at most with one charge carrier.]

Qualitatively similar effects of positional disorder on T_c are found for higher Mn concentrations as well as higher hole densities, although the effects are quantitatively substantially less (see Fig. 3 from Ref. 18). All the curves shown so far correspond to one particular disorder realization. As the amount of the disorder increases, so do the variations between curves obtained for different disorder realizations. In Fig. 6 we show typical results for 25 different disorder realizations for $x=0.05$. These significant variations demonstrate the degree of sensitivity, in this model, to the particular arrangement of Mn dopants. This is to be contrasted with the
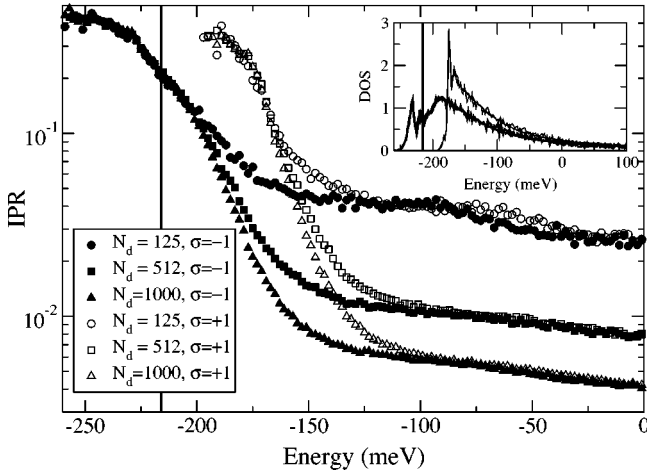
FIG. 7. Average IPR as a function of energy for subbands with $\sigma=\downarrow$ (full symbols) and $\sigma=\uparrow$ (empty symbols) of completely random Mn distributions with $p=10\%$, $x=0.009\,26$, and $N_d=125$ (circles), 512 (squares), and 1000 (triangles). The vertical line marks the Fermi level. All occupied states are localized. The inset shows the total density of states for the two subbands (arbitrary units).

results of a homogeneous model which neglects Coulomb interactions, where curves corresponding to different disorder realizations are indistinguishable (for example, Fig. 2 of Ref. 21).

C. Metal-insulator transition

According to Mott's criterion, a doped semiconductor goes through a metal-insulator transition (MIT) for a charge-carrier concentration given by $n_h^{1/3}a_B\sim 0.25$. (For compensated systems, the critical density is experimentally found to be somewhat larger.) Neglecting the effects of compensation and assuming $p=10\%$ and $a_B=7.8$ Å, the MIT corresponds to $x\sim 0.02$. This estimate agrees with the experimental value of $x\sim 0.03$.[27]

A way of finding the MIT is by determining the nature (localized or extended) of the charge-carrier states near the Fermi level. This is defined by the inverse participation ratio (IPR) given for each state ($n\sigma$) by

$$IPR(n\sigma)=\frac{\sum_i |\psi_{n\sigma}(i)|^4}{\left(\sum_i \left|\psi_{n\sigma}(i)\right|^2\right)^2}.$$

For a state extended over the N_d sites of the system, one expects $|\psi_{n\sigma}(i)|\sim 1/\sqrt{N_d}$, leading to $IPR(n\sigma)\sim 1/N_d$. It follows that for extended states, $IPR(n\sigma)$ is inversely proportional to the size of the system. For localized states, $IPR(n\sigma)$ is inversely proportional to the number of sites over which the wave function is localized, and thus independent of the size of the system.

In Fig. 7 we plot $IPR(E,\sigma)$ for a completely disordered system with $x=0.009\,26$ and $p=10\%$ in the limit $k_BT\rightarrow 0$. For each system size we study 100 different disorder realiza-
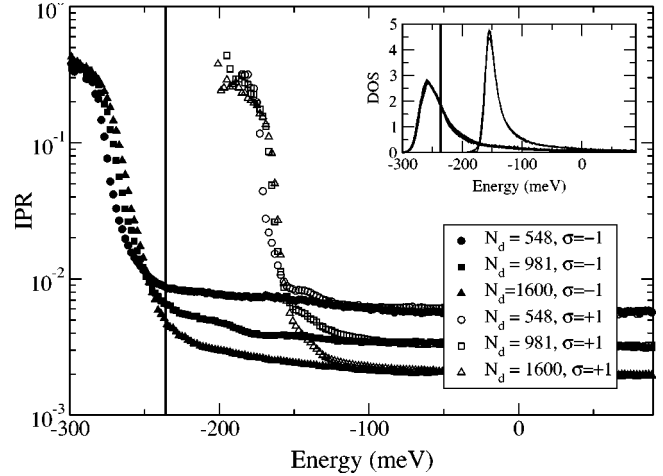

FIG. 8. Average IPR as a function of energy for the $\sigma=\downarrow$ (full symbols) and $\sigma=\uparrow$ (empty symbols) subbands of completely random Mn distributions with $p=10\%$, $x=0.05$, and $N_d=548$ (circles), 981 (squares), and 1600 (triangles). The vertical line shows the Fermi energy, above the mobility edge. The inset shows the DOS for the two subbands, in arbitrary units.

tions and average the IPR of all the states with eigenvalues within 2 meV of each other. We show both the $\sigma=\downarrow$ and $\sigma=\uparrow$ subbands for three system sizes, $N_d=125,512$, and 1000, corresponding to $N_h=12,51$, and 100. A large gap of size $4.2J=63$ meV opens between the two subbands, and only states in the $\sigma=\downarrow$ are occupied at this low temperature. The states at the bottom of either band are localized, with the IPR independent of the system size. At higher energy, however, the states become extended, with the $IPR\sim 1/N_d$. The mobility edge for the $\sigma=\downarrow$ band is at an energy of about -200 meV. The Fermi level (marked by the vertical line, at about 45 meV above the bottom of the band), is below the mobility edge; this implies insulating behavior, in agreement with experimental measurements. However, the IPR of the states at the Fermi energy is less than a factor of 2 larger than the IPR at the mobility edge. This suggests that significant tunneling occurs between various regions occupied by charge carriers, helping the alignment of magnetization of all the polarized regions. The inset shows the DOS for the two subbands. The DOS has an extremely long upper tail, only part of which is shown (for discussions, see Appendix). For this small $p=10\%$, only states close to the bottom of the impurity band are occupied, justifying the neglect of the band states. The histograms presented in Fig. 5(a) indicate that at higher T, the distribution of charge carriers becomes somewhat more homogeneous. This suggests that the charge-carrier wave functions become more extended at higher T, i.e., the system is more "metallic." This is in qualitative agreement with resistivity measurements[27] which show a larger resistivity at low temperatures than above T_c for all low-density samples.

IPR curves for $x=0.05$ and completely random disorder are shown in Fig. 8. In this case, we use larger size systems ($N_d=548,981$, and 1600) to avoid finite-size effects. Again, states at the bottom of either subband are localized, while states at higher energies are extended (their IPR scales with $1/N_d$). In this case, the system is clearly above the metal-
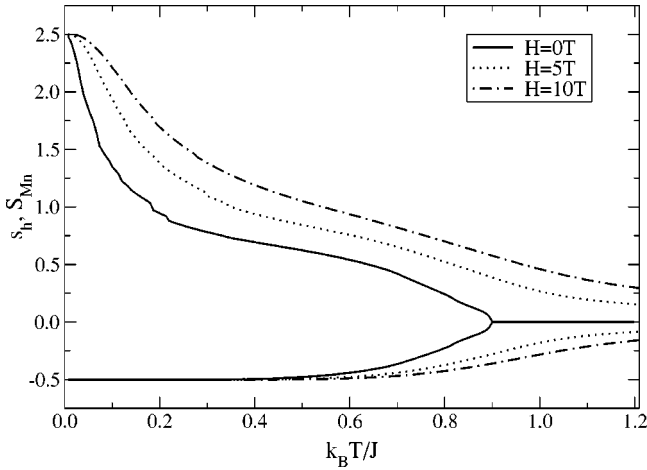
FIG. 9. Mn and charge-carrier magnetizations as a function of T for a random Mn configuration with $x=0.05$ and $p=10\%$, and external magnetic field $H=0,5$, and 10 T. The overall magnetization is significantly increased at all T.

insulator transition, in qualitative agreement with experiment. Experimentally it was observed[4,13,27] that samples with higher concentrations ($x>0.07$) show reentrant insulating behavior. However, these samples also have a much lower charge-carrier density. Since the $x=0.05$ system is just above the MIT, it is reasonable to assume that a large decrease in the density of charge carriers will move the Fermi level below the mobility edge and thus lead to insulating behavior. This agrees with recent experiments[6] which show that proper annealing of such samples, which increases their hole concentrations, leads to metallic behavior.

The fact that these systems are either metallic, or not too far from the MIT, is important for obtaining a large T_c. Maximizing the critical temperature seems to require a fine balance: increasing the disorder leads to increased T_c, but also to increased localization. If the charge-carrier states become so localized that there is no tunneling in between high-density regions, than the directions of polarization of such regions become uncorrelated, and the average magnetization vanishes ($T_c \rightarrow 0$).

D. Effects of external magnetic fields

We now consider the effect of an external magnetic field, in the absence of on-site interactions $u(i)=0$. We take $\tilde{g}=2$ for the Mn spins. The precise value of the g factor for the holes is not important, since we find that the magnetization is not changed if we vary g within a reasonable range. This is a consequence of the fact that each hole strongly interacts with many Mn spins, and the external magnetic field is just a small perturbation to the effective on-site energy $\epsilon_{i\sigma}$ experienced by holes [see Eq. (7)]. On the other hand, the external magnetic field leads to a significant change in the effective magnetic field H_i [see Eq. (4)] of each Mn spin, since each Mn spin interacts with very few holes. In Fig. 9 we plot the magnetization of a disordered configuration with $x=0.05$ and $p=10\%$, in the presence of an external magnetic field $H=0,5$, and 10 T. The external
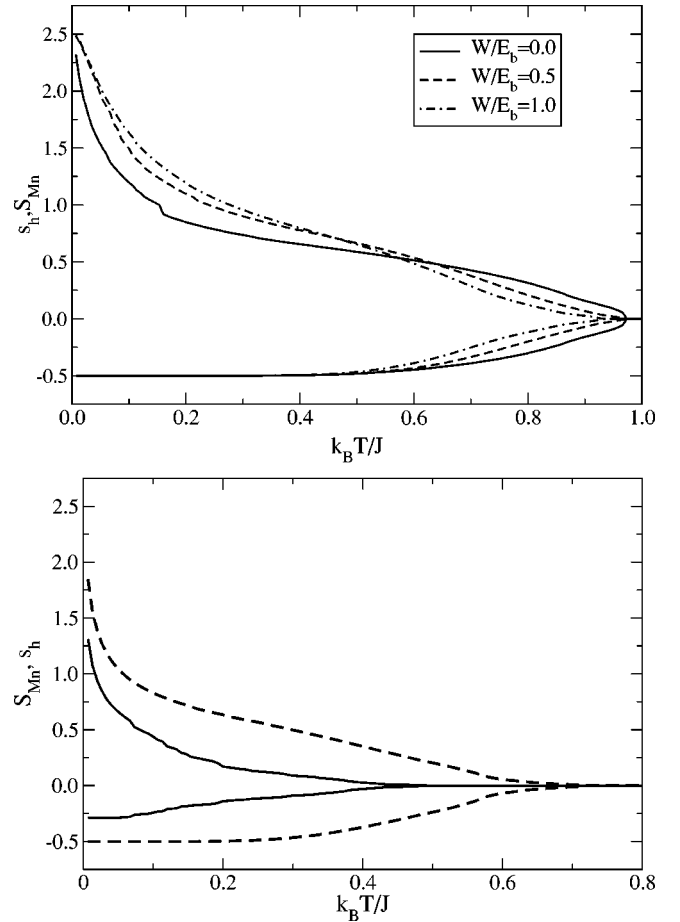

FIG. 10. (a) Mn and charge-carrier magnetizations for a random Mn configuration with $x=0.05$ and $p=10\%$, and an on-site disorder cutoff $W/E_b=0,0.5$ and 1; (b) Magnetization curves without (dashed), and with (full line) an on-site interaction with As antisites, explained in text. Both curves are for the same disorder realization, $x=0.009\,24$ and $p=10\%$.

magnetic field leads to a significant increase of the Mn spin magnetization at all T, since it polarizes the many weakly interacting spins. It also leads to a saturation of the magnetization for temperatures $k_B T < g\mu_B H$, as expected. The magnetization of the charge carriers is also increased (in magnitude) in the presence of the magnetic field. This may seem puzzling, since the external magnetic field should favor a flip of the charge-carrier spin from $\sigma=\downarrow$ to $\sigma=\uparrow$. However, as the magnetization $S_{Mn}(i)$ of each Mn spin increases with H, the effective negative magnetic field felt by charge carriers increases, more than compensating the Zeeman contribution from H [see Eq. (7)].

E. Effects of on-side disorder

We now consider the effect of the on-site disorder $u(i)$ in this model. While the nature of the heavy compensation is not fully elucidated at this point, it is due to some type of charged defects. These create an electric potential $u(i)$ at all Mn sites. The simplest way to describe it is to assume that the on-site energies $u(i)$ are distributed with equal probability in the interval $[-W,W]$. In Fig. 10(a) we compare the

average Mn and spin charge-carrier magnetizations obtained from a random Mn configuration with $x=0.05$ and $p=10\%$, for various values of the on-site disorder cutoff $W/E_b=0,0.5$, and 1. On-site disorder does not affect T_c considerably (in all cases we find that T_c decreases slowly with increasing W) but changes the shape of the magnetization curve. It is interesting to note that the magnetization of the sample with $W=1$ Ry varies almost linearly with T. Such unusual $M(T)$ dependence has been observed experimentally.[4,28]

We also investigated a more detailed model for on-site disorder, assuming that compensation is entirely due to As antisites. If a valence-V As atom substitute for a valence-III Ga atom, the two extra valence electrons effectively remove two holes from the impurity band. If all compensation is due to such processes, the number of As antisites is given by $N_{As}=N_d(1-p)/2$. Each such As impurity has an effective charge $+2e$, and will contribute an on-site Coulomb potential $+2e^2/\epsilon r$ for a Mn impurity which is a distance r away. One could use a detailed formula $u(i)=-\Sigma_j e^2/\epsilon r_{j,Mn}+\Sigma_k 2e^2/\epsilon r_{k,As}$, where the first (second) term describe the Mn (As antisite) contributions. A simpler way is to assume that each As antisite only contributes to the on-site potential $u(i)$ of its two nearest Mn neighbors, with the contribution to more distant Mn sites being screened out by the two nearest Mn sites. The two formulations are qualitatively equivalent; we investigate the simpler one. In this case, after we randomly choose locations for the Mn impurities, we select random positions on the Ga sublattice for the As antisites. We find the two closest Mn neighbors for each As antisite (each Mn is neighbor to only its closest As antisite), compute the corresponding values for $u(i)$ and then proceed with the calculation as described previously. Typically, the on-site interaction in this model leads to a substantial decrease in T_c [see Fig. 10(b)]. Also, the shape of magnetization curves becomes even more concave and the hole magnetization no longer reaches saturation in the $T=0$ limit. We conclude that on-site disorder leads to an overall decrease of T_c.

F. Beyond the hydrogenic model

As emphasized in the introduction, the impurity band model with hydrogenlike, exponentially decaying hopping neglects many aspects of the full Hamiltonian for a system like $Ga_{1-x}Mn_xAs$, especially with large numbers of As antisite defects and/or interstitial Mn defects.[20] First, the Mn dopant is not exactly "shallow," with a binding energy of over 100 meV. This suggests that the true wave function is substantially affected by central cell corrections, which could affect the hopping integrals considerably. Second, the magnitude of $t(r)$ is based on a two-center approximation for spherically symmetric wave functions (see Appendix). Besides the obvious complication of anisotropy of the true hole wave function, these could lead to substantial renormalization of the effective $t(r)$ at the densities of interest, especially at the upper end (few percent). More microscopic calculations[11] suggest a significant renormalization of the energies within the impurity band, compared to the simple two-center tight-binding picture. Consequently, we discuss the

effects of changing the hopping parameter $t(r)$ below. The effect of other approximations made, such as the neglect of carrier-carrier interactions and the valence-band states, are discussed following that.

A decrease of the magnitude of the hopping can be achieved by changing the Bohr radius, or the prefactor. A change in Bohr radius is merely a renormalization of the effective density, while the effect of changing the prefactor is tantamount to changing the exchange coupling in the opposite direction, and then rescaling the temperature scale appropriately. To study the effects of restricting the hopping to nearby sites only, we investigated a model where hopping is limited to sites within a radius r_h. One expects r_h to decrease with density, so as to maintain a reasonable coordination number, $z=(4\pi/3)n_{Mn}r_h^3$. We use a phenomenological formula $z=12n_{Mn}/(n_c+n_{Mn})$, where n_c is the Mn concentration for which the density of holes $n_{MI}=pn_c$ corresponds to the metal-insulator transition $n_{MI}^{1/3}a_B=0.25$. This formula has the proper asymptotic limits: z is proportional to n_{Mn} at low density and saturates to $z=12$ at large n_{Mn}, whereas $z=6$ at the MIT.[11] We obtain $r_h=2.22a_B$ for $x=0.0092$ corresponding to an average $z=4.7$, whereas for $x=0.05$ we have $r_h=1.59a_B$ and $z=9.23$.

Another issue concerns the sign of the hopping integral. In the model studied, all hopping integrals have the same sign, namely, the one for which the density of states near the band edge where the relevant physics takes place has a position, width, and a mobility edge, in agreement with physical expectations (for more details, see Appendix and Ref. 29). However, the real system is heavily compensated and the repulsive potentials due to these compensating centers may change the sign of some hopping elements. In an effort to see the influence of such effects, we have also studied models where $t(r)$ has random signs.

Figure 11 shows magnetization curves obtained for various models, as described in the caption. Details of the hopping parameter lead to different T_c; consequently we show the data on a scaled plot in terms of T/T_c. The crucial issue appears to be the density of states near the Fermi level. Impurity bands that are broad have low T_c, while those that are relatively narrow, as might be expected for centers that have a strong central cell or on-site exchange energy, have high T_c. Despite the variation in T_c, we find a number of features that are generic to all the models studied, as illustrated in Fig. 11:

(a) For each $t(r)$ studied, *within the mean-field approximation* the T_c of the disordered system is higher than that of the corresponding ordered superlattice, while the magnetization at low T (below $T_c/3$ or so) is lower.

(b) The magnetization curves obtained with impurity bands from a set of positional disordered impurity centers have an unusual concave shape compared to the standard convex magnetization of most uniform magnets.

(c) There is significant temperature dependence of $M(T)$ for $T \ll T_c$, unlike in essentially uniform magnetic systems where the magnetization reaches its $T=0$ saturation value around $T_c/2$ or $T_c/3$.
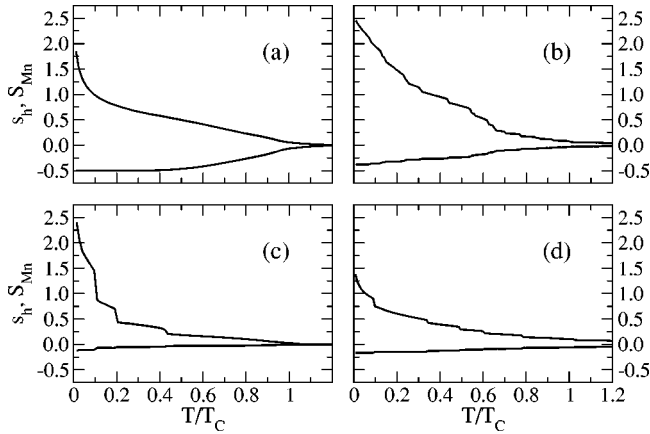
FIG. 11. Mn and charge-carrier magnetizations as a function of T/T_c for *one* random Mn configuration with $x=0.009\,26$ and $p=10\%$. Curves are for: (a) hopping between all sites, same-sign hopping integral ($T_c/J\sim0.6$); (b) hopping only for sites within $r_h=2.22a_B$ of each other, same-sign hopping integral ($T_c/J\sim0.2$); (c) hopping between all sites, random-sign hopping integral ($T_c/J\sim0.12$); (d) hopping only for sites within $r_h=2.22a_B$ of each other, random-sign hopping integral ($T_c/J\sim0.2$). Sample averaging is required to obtain smooth curves. For more details, see text.

(d) Some of the unusual features of the Mn spin curves, which determine the bulk magnetization, are seen in the hole magnetization curves as well (see Fig. 11).

Other approximations made in our study involve neglecting a number of complications present in the system such as: (i) the detailed effects of the compensating centers, (ii) carrier-carrier interactions, and (iii) the valence-band states. For (i) we have considered (Sec. III E) one of the effects, namely, addition of an effective on-site random potential for the extreme cases where the on-site potential is either uncorrelated, or modeled as being due to a close by As antisite defect. However, the Coulomb potentials from these centers could also affect the hopping parameters, as we discussed in the preceding paragraphs and in the Appendix. The states near the Fermi level for the range of concentrations we consider are not strongly localized in the model studied, and in fact the actual system is fairly close to a MIT. Consequently, we believe that approximation (ii) is reasonable. Since electron-electron interactions are partially screened (see Appendix), the simplest description involves an on-site interaction U as in the Hubbard model. Within mean-field approximation, such a term will increase T_c, since it aids in the splitting of the up and down spin bands. This expectation is indeed confirmed (see Fig. 12), with an increase in T_c of about 35% for the $x=0.01$ case and 18% for the $x=0.05$ case for a value $U=1$ Ry typical for hydrogenic centers at low densities. This is likely an overestimate, since the effective U near the metal-insulator transition is likely to be reduced by screening processes.

Finally, we discuss the neglect of the valence-band states. In this model this is not important, at least at low T, where the shape of the magnetization is anomalous and where the mean-field results are at least qualitatively correct. This is because the Fermi level lies ~2–300 meV above the valence-band minimum, and excitations to the valence-band
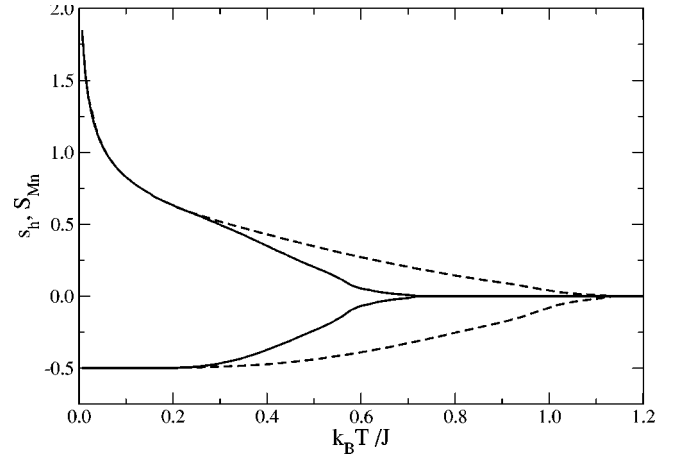

FIG. 12. Effect of an electron-electron on-site interaction $U=1$ Ry (treated within the mean-field approximation) on the magnetization curves for $x=0.01$ and $p=10\%$ (dashed curve). Full line is the same curve, but for $U=0$.

states are important only at very high temperatures. It should also be emphasized that the impurity states that we consider are derived from the host band (the valence band for $Ga_{1-x}Mn_xAs$). Consequently, if one wishes to include the rest of the band states of the host, they must be orthogonalized to the impurity states; this has the effect of pushing the host band even further from the impurity band. In a more realistic model, however, this remains an open question.

IV. SUMMARY AND CONCLUSIONS

We studied a simplified model of III-V DMS, with charge carriers restricted to a band formed from impurity orbitals, as in shallow doped semiconductors. We believe that this is a good starting point, especially for low concentrations, because the high compensation present in these systems leads to carrier densities which are not large enough to fully screen out the Coulomb interaction between the Mn ions and the charge carriers. This is clearly indicated by the metal-insulator transition inside the range of dopings of interest ($x=1$–5 % Mn).

We first analyze the ordered superlattice, with a homogeneous charge-carrier distribution. We then show that positional disorder and on-site random interactions lead to significant changes in the shape of the magnetization and the critical temperature T_c. This enhancement of T_c has already been confirmed by Monte Carlo simulations, although the overall increase is smaller than predicted by mean field.[24] It should also be emphasized that the exchange coupling we use (from Ref. 9) is lower than the values used by MacDonald *et al.*[8] or Millis and Das Sarma[30] to obtain similar T_c. The reason for this is that our impurity wave functions are peaked at the Mn sites, leading to greater charge density at the Mn sites than for host band wave functions.

We have not performed detailed numerical fits to T_c because of a number of factors, such as (a) the complicated nature of the hole wave functions, (b) uncertainties about the nature of the compensation processes, (c) uncertainties about the precise description of the hopping integral, (d) the under-

estimation of the effect of thermal fluctuations by the mean-field approximation, etc. One of the robust results that follows from our study is that the magnetization curves $M(T)$ may vary considerably from the canonical concave downward form seen in practically all uniform magnetic models, independent of dimension or spin components. Using different hopping parameters, we find that while T_c changes with the model chosen, the concave-upward form of $M(T)$ over much of the temperature range below T_c is dependent mostly on the Mn spin concentration x and the carrier density px. The curves vary from essentially concave functions (as reported in Ref. 1) for large relative charge-carrier concentrations p, to almost linear dependence (as reported in Ref. 4), to very concave upward functions (as reported in Ref. 12) as p is decreased. Below T_c, our magnetization curves generically show a fast increase, followed by saturation and then fast increase again at much lower temperature, similar to reports in Ref. 13. Overall, we claim good qualitative agreement with the experimental behavior concerning possible shapes of magnetization curves, the MIT etc. Our study suggests that by appropriate tuning of parameters, one may tailor the magnetic behavior $M(H,T)$ in a manner not possible in simple uniform magnets.[31] We believe that detailed information provided by experiments (using local probes such as electron spin resonance and nuclear magnetic resonance) would allow a clearer understanding of the nature of ferromagnetism in these compounds.

Returning to the issue of the magnitude of T_c, we believe the most important correction to our mean-field result is due to thermal (temporal) fluctuations, which are not included in a mean-field treatment. While typical renomalizations of T_c for uniform ferromagnets range from tens of percent to factors of 2 or so, we expect them to be significantly larger for models such as this with great spatial inhomogeneity, where percolation aspects have considerable influence. Indeed, Monte Carlo simulations[24] show that T_c is significantly suppressed with respect to the mean-field value, especially for the lower concentrations x and p, where the magnetization is less robust. Different theoretical approaches have also confirmed the increase of T_c with disorder.[32] In addition to fluctuation effects, there are interactions not included in our model which may lead to an overall decrease of T_c *even within mean field*. One example is the direct Mn-Mn spin interactions. They are expected to be AFM, as in II-VI DMS.[33] This may lead to frustration, especially in the high-concentrations regions (which determine the value of T_c in our model) where Mn-Mn interactions are the largest. In particular, nearest-neighbor Mn spins may lock in a singlet state, and therefore not contribute at all to magnetization. Spin-orbit coupling, also absent in our model, has recently been shown[34] to result in anisotropic exchanges which lead to frustration and decrease of T_c.

APPENDIX THE HOPPING MATRIX

For consistency purposes, we perform a particle-hole transformation, and work in an ''electron'' formalism. In other words, we assume that Mn atoms are donors (not acceptors) and the charge carriers are electrons occupying an impurity band located below the conduction band.

1. General formulation of hopping problem

Consider a system containing N dopant atoms (Mn) located at sites $\vec{R}_i$, $i=1,\ldots,N$, as well as some other type of charged impurities responsible for compensation, located at positions $\vec{R}_\alpha$, $\alpha=1,\ldots,N_i$. In the absence of electron-electron interactions, the Hamiltonian is

$$\mathcal{H}=T+\sum_{i=1}^{N} V_i(\vec{r})+\sum_{\alpha=1}^{N_i} U_\alpha(\vec{r}), \qquad (A1)$$

where T describes the kinetic energy of the electron, and $V_i(\vec{r})<0$ and $U_\alpha(\vec{r})>0$ are the interaction of the electron with the ith dopant and αth charged impurity. For a single dopant, the ground state is a shallow level localized about the Mn site, given by $\mathcal{H}_i\phi_i(\vec{r})=[T+V_i(\vec{r})]\phi_i(\vec{r})=E_i\phi_i(\vec{r})$.

In an impurity band model, we restrict the Hilbert space to that spanned by the ground-state wave functions of all dopants, $\Psi(\vec{r})=\Sigma_{i=1}^N\alpha_i\phi_i(\vec{r})$. The Schrödinger equation for Hamiltonian (A1) becomes

$$\sum_{j=1}^{N} \mathcal{H}_{ij}\alpha_j=E\sum_{j=1}^{N} \mathcal{O}_{ij}\alpha_j, \qquad (A2)$$

where

$$\mathcal{H}_{ij}=\langle\phi_i|\mathcal{H}|\phi_j\rangle; \quad \mathcal{O}_{ij}=\langle\phi_i|\phi_j\rangle. \qquad (A3)$$

For a random collection of impurities $\mathcal{O}_{ij}\neq\delta_{ij}$. Let $\mathcal{O}^{-1}$ be the inverse of $\mathcal{O}$, and $H=\mathcal{O}^{-1}\mathcal{H}$. Now Eq. (A2) can be recast in the standard form $\Sigma_{j=1}^N H_{ij}\alpha_j=E\alpha_i$ corresponding to the hopping Hamiltonian

$$\mathcal{H}_{hopping}=\sum_{i=1}^{N} H_{ii}a_i^\dagger a_i+\sum_{i\neq j} H_{ij}a_i^\dagger a_j \qquad (A4)$$

and a wave function $|\Psi\rangle=\Sigma_{i=}^N\alpha_i a_i^\dagger|0\rangle$. Here, $a_i^\dagger$ is the creation operator for an electron in the impurity level of the ith dopant, satisfying the usual anticommutation relations $\{a_i,a_j^\dagger\}=\delta_{ij}$. The spin can be added trivially.

Thus, the hopping integral between sites i and j is

$$t_{ij}=H_{ij}=\sum_{k=1}^{N} \mathcal{O}_{ik}^{-1}\mathcal{H}_{kj}. \qquad (A5)$$

2. Hopping matrix between two isolated impurities

Consider a system which contains only two identical dopant atoms $\mathcal{H}=T+V_1+V_2$. Then, the hopping matrix is a function only of the distance $R=|\vec{R}_1-\vec{R}_2|$ between the two impurities given by [see. Eq. (A5)]

$$t(R) = \frac{\langle\phi_1|V_1|\phi_2\rangle - \langle\phi_1|\phi_2\rangle\langle\phi_2|V_1|\phi_2\rangle}{1 - \langle\phi_1|\phi_2\rangle\langle\phi_2|\phi_1\rangle}. \qquad (A6)$$

For a Coulomb interaction $V_i(\vec{r}) = -e^2/|\vec{r} - \vec{R}_i|$, the impurity wave function is $\phi(r) = 1/\sqrt{\pi a_B^3}\exp(-r/a_B)$ and the various matrix elements can be computed *exactly*

$$\langle\phi_1|V_1|\phi_2\rangle = t_0(R) = -2\left(1 + \frac{R}{a_B}\right)e^{-R/a_B} \quad \text{Ryd,}$$

$$\langle\phi_1|\phi_2\rangle = \left[\frac{1}{3}\left(\frac{R}{a_B}\right)^2 + \frac{R}{a_B} + 1\right]e^{-R/a_B},$$

$$\langle\phi_2|V_1|\phi_2\rangle = -\frac{2a_B}{R}\left[1 - \left(1 + \frac{R}{a_B}\right)e^{-2R/a_B}\right] \quad \text{Ryd.}$$
$$(A7)$$

This gives $t(R) = t_0(R)f(R/a_B)$, where $t_0(R)$ is defined in Eq. (A7) and the rescaling function

$$f(x) = \frac{1 - \dfrac{1}{x(x+1)}\left[1 + x + \dfrac{x^2}{3}\right]\left[1 - e^{-2x}(1+x)\right]}{1 - e^{-2x}\left[1 + x + \dfrac{x^2}{3}\right]^2}$$

is such that $\lim_{x\to 0}f(x) = 1$ and $\lim_{x\to\infty}f(x) = \frac{2}{3}$.

For a real donor/acceptor, the Coulomb potential is always supplemented by a central-cell correction; this supplementary potential modifies both the Rydberg and the shape of the wave function. Thus, the simple formula for $t(R)$ found above does not generally hold. However, one can still define a Bohr radius to characterize the exponential decay of the true wave function far from the impurity,[10] and therefore one expects exponential decay of the hopping matrix at large R. As a result, it is customary to use the simpler $t_0(R)$ as the hopping integral,[11] with the "true" Ryd and a_B values. Obviously, the whole $t(R)$ formula can equally well be used, but this leads to only small quantitative differences.

3. Many impurities

In this case, one should obtain the hopping matrices from Eq. (A5). For N impurities this means computing $N(N-1)$ matrix elements for $\mathcal{H}$ and $\mathcal{O}$, a matrix inversion and a matrix multiplication. If detailed information about the system is known, such a procedure can be followed. However, for systems with considerable uncertainty about the nature of the compensation [the shape and location of potentials $U(\vec{r})$, plus the central cell corrections to $V(\vec{r})$] such a procedure is not warranted, since the matrix elements cannot be accurately modeled. Instead, it is customary to use $t_0(R)$ to describe the hopping between any two sites. This prescription obviously implies a number of major approximations. Most importantly, it completely neglects the existence of the impurities responsible for compensation [the potentials $U(\vec{r})$], with significant effects, as described below.

Let us assume that the hopping between any two sites is indeed given by $t_0(R)$, and that the donor atoms are located on a cubic ordered superlattice (there is no disorder). Then, the Hopping Hamiltonian is diagonalized by plane waves, leading to a dispersion relation for the impurity band

$$\epsilon(\vec{k}) = \sum_{i\neq 0} t(r_i)e^{i\vec{r}_i\cdot\vec{k}}. \qquad (A8)$$

For $t < 0$, the lower band edge is at $\vec{k} = (0,0,0)$ (center of the Brillouin zone) and is given by $\epsilon_{min} = \Sigma_{i\neq 0}t(r_i)$. Although $t(r)$ decrease exponentially, the number of neighbors at r increases roughly like r^2 (surface of a sphere). Thus, a very large number of contributions are added to ϵ_{min} before convergence is reached. Numerically, we find that (depending on x) convergence is sometimes still not reached in systems with as many as 512 dopants, showing that sizable contributions to ϵ_{min} are still coming from even further away sites. Summing such a large number of contributions gives a very negative value for ϵ_{min} (several electron volt). The DOS near this band edge is extremely low, since for any finite but small $\vec{k}$, sites for which $\vec{r}_i\cdot\vec{k} > \pi$ will contribute with the opposite sign to $\epsilon(\vec{k})$ [Eq. (A8)] and will have energies significantly larger than ϵ_{min}. To summarize, this means that the bottom of the impurity band has a very long tail down to very low energies.

This picture is clearly wrong. Such a big negative value for ϵ_{min} places the bottom of this impurity band (i.e., the states occupied by the doping electrons) well inside the valence band itself, as opposed to somewhere inside the gap (the gap is typically ~ 1 eV). Even if this problem is disregarded, if the doping electrons occupy such a long tail, it follows that disorder in the dopant positions and/or any other interactions have basically no effect on the physics of the system. The reason is simply that the energy scales associated with any other interactions/disorder are much smaller than the huge energy scale $|\epsilon_{min}|$, and thus any other interactions are in effect tiny perturbations. For instance, disorder-induced localization is expected if the kinetic energy lost by the electron through localization is compensated by stronger interactions of the electron within the localization area. Clearly, this can never happen for states in this long tail, where the kinetic energy is so huge that it becomes impossible to overcompensate. It follows that states in this "impurity band" are always delocalized throughout the entire system, contrary to physical expectations. Magnetic interactions such as we consider in this paper will also have basically no effect on the system. Even in the most optimum case, where all Mn spins are fully polarized, such an interaction only opens a gap on the order of JS between spin-down and spin-up subbands. This is minuscule compared to the scale of ϵ_{min} (comparable to the Fermi energy, due to the small density of states) and it will fail in producing any charge-carrier polarization.

The absence of ferromagnetism as well as the strong size-dependent effects for this model for $t < 0$ has been commented upon in Ref. 35 [the absence of localization and of a mobility edge was demonstrated in Ref. 29]; as a result, its authors advocate that impurity band models are not relevant for study of III-V DMS. However, it is clear that the problem

is much more serious, since this analysis suggests that the impurity band approach should never be used (unless x is orders of magnitude smaller than 1%) due to the presence of this long tail at very low energies. This is an unacceptable conclusion.

The reason for this unphysical behavior can be easily traced back to the simplified form $t_0(R)$ used for the hopping. This form implies that an electron always feels the $V(\vec{r})$ attraction from any other dopant site, no matter how far away it is. This leads to the slow exponential decay of $t(R)$, the resulting slow convergence of the sum for ϵ_{min} and thus its large absolute value. However, real systems are electrically neutral; an electron should feel no overall attractions/ repulsions from regions of the sample far from it. Neutrality is achieved by including the effect of the charged (repulsive) impurities responsible for compensation, as well as the effect of other electrons in the system. Since both $V(\vec{r})$ and $U(\vec{r})$ terms must be included in the matrix elements [see Eqs. (A1)–(A5)], it follows that the attraction from a far away dopant may be more than compensated for by the presence of a charged impurity nearby. At the very least, this will decrease the size of the hopping matrix, but it may well give it an opposite sign or set it to zero. Also, if an electron is trapped on a far-away site, the attraction potential from that dopant is canceled by repulsion from the electron. If one thinks of the effect of other electrons in terms of a screening of the potentials V and U, it is apparent that there can be no hopping to sites at distances larger than the screening length. If we use the Thomas-Fermi approximation (certainly not valid here), we find a screening length of the order of 10 Å for densities of interest; depending on x, around ten dopants are inside this screening length from any given site and contribute to ϵ_{min}. This is a huge change from the more than 500 dopants found to contribute to ϵ_{min} if charge neutrality is ignored. All these effects lead to a significant renormalization of the energy scale ϵ_{min} to more physical values (a few Ry) and a corresponding increase of the density of states near the bottom of the impurity band. As soon as this energy scale takes reasonable values, the system will be strongly influenced by disorder and other interactions with comparable energy scales.

The question then is how to fix the problem of this unphysical tail leading to unphysical results. As already stated, the computational effort suggested by Eqs. (A1)–(A5) (which should be supplemented by the contribution of the electron-electron interactions) is not warranted if there is significant uncertainty regarding the exact nature of the compensation processes. *Ad hoc* schemes, such as limiting hopping only to nearest-neighbor sites (in the Wigner-Seitz sense), have been used in literature,[11] but they are hard to justify quantitatively. As a result, we use a different approach. We first note that the upper band edge of the impurity band does not exhibit this anomalous behavior. For the ordered lattice, this band edge corresponds to $\vec{k}=(\pi,\pi,\pi)$, and contributions from consecutive neighbors to ϵ_{max} come with alternating sign, leading to partial cancellations. The sum converges much faster and finite-size effects at this band edge are absent even for system with as few as 100 dopants (we have not investigated smaller systems). This partial cancellation also leads to a reasonable value of $\epsilon_{max}>0$, of 2–3 Ry. As a result, in the presence of disorder the states near this band edge become localized,[29] and a mobility edge separates them from extended states close to the center of the band. The DOS and position of this band edge is not much changed by proper consideration of the system neutrality, since that influences significantly only contributions from far-away sites, which for ϵ_{max} are canceled. In effect, this upper band edge has all the correct, physically expected behavior absent in the anomalous lower band edge. We therefore choose the simplest route to fixing the problem, which is to take $t>0$. Inversion of the sign simply interchanges the two band edges (similar to a particle-hole transformation) and all occupied states are now at reasonable energies inside the gap and in the vicinity of a mobility edge. Magnetic interactions also become relevant, as shown throughout the paper.

The final question is why should this simple scheme work well. Qualitatively, all the effects of disorder that we uncover are related to localization of the electrons at the bottom of the impurity band. This is the expected behavior physically, since the system is close to a MIT transition, and it is well captured in this scheme. As discussed in Sec. III F, other *ad hoc* schemes for the impurity band lead to the same qualitative physics, *if* the occupied states are near a mobility edge. Quantitatively, there is no *a priori* reason why the simple scheme of inverting the sign of t should work best. However, we obtain reasonable (order of magnitude) estimates for T_c, as well as the position of the MIT, without any parameter adjusting. This encourages us to believe that this simple impurity band model is accurate enough to be used for first-order computations regarding such systems. Further study of this problem is being pursued.

---

[1] H. Ohno, J. Magn. Magn. Mater. **200**, 110 (1999).

[2] H. Ohno, A. Shen, F. Matsukura, A. Oiwa, A. Endo, S. Katsumoto, and Y. Iye, Appl. Phys. Lett. **69**, 363 (1996).

[3] T. Hayashi, M. Tanaka, T. Nishinaga, H. Shimada, H. Tsuchiya, and Y. Otsuka, J. Cryst. Growth **175**, 1063 (1997).

[4] A. Van Esch, L. Van Bockstal, J. De Boeck, G. Verbanck, A.S. van Steenbergen, P.J. Wellmann, G. Grietens, R. Bogaerts, F. Herlach, and G. Borghs, Phys. Rev. B **56**, 13 103 (1997).

[5] K.W. Edmonds, K.Y. Wang, R.P. Campion, A.C. Neumann, N.R.S. Farley, B.L. Gallagher, and C.T. Foxon, Appl. Phys. Lett. **81**, 4991 (2002).

[6] S.J. Potashnik, K.C. Ku, R. Mahendiran, S.H. Chun, R.F. Wang, N. Samarth, and P. Schiffer, Phys. Rev. B **66**, 012408 (2002).

[7] T. Dietl, A. Haury, and Y.M. d'Aubigné, Phys. Rev. B **55**, R3347 (1997); M. Takahashi, *ibid.* **56**, 7389 (1997); T. Dietl, H. Ohno, F. Matsukura, J. Cibert, and D. Ferrand, Science **287**, 1019 (2000).

[8] J. König, H.-H. Lin, and A.H. MacDonald, Phys. Rev. Lett. **84**,

5628 (2000).

[9] A.K. Bhattacharjee and C.B. à la Guillaume, Solid State Commun. **113**, 17 (2000).

[10] B.I. Shklovskii and A.L. Efros, *Electronic Properties of Doped Semiconductors* (Springer-Verlag, Berlin, 1984).

[11] R.N. Bhatt and M.T. Rice, Phys. Rev. B **23**, 1920 (1981).

[12] B. Beschoten, P.A. Crowell, I. Malajovich, D.D. Awschalom, F. Matsukura, A. Shen, and H. Ohno, Phys. Rev. Lett. **83**, 3073 (1999).

[13] S. Katsumoto, A. Oiwa, Y. Iye, H. Ohno, F. Matsukura, A. Shen, and Y. Sugawara, Phys. Status Solidi B **205**, 115 (1998).

[14] J. Okabayashi, A. Kimura, O. Rader, T. Mizokawa, A. Fujimori, T. Hayashi, and M. Tanaka, Physica E (Amsterdam) **10**, 192 (2001).

[15] B. Grandidier, J.P. Nys, C. Delerue, D. Stievenard, Y. Higo, and M. Tanaka, Appl. Phys. Lett. **77**, 4001 (2000).

[16] H. Asklund, L. Ilver, J. Kanski, J. Sadowski, and R. Mathieu, Phys. Rev. B **66**, 115319 (2002).

[17] Y. Nagai, T. Kunimoto, H. Nojiri, M. Motokawa, F. Matsukura, T. Dietl, and H. Ohno, Jpn. J. Appl. Phys. **40**, 6231 (2001); E.J. Singley, R. Kawakami, D.D. Awschalom, and D.N. Basov, Phys. Rev. Lett. **89**, 097203 (2002).

[18] Mona Berciu and R.N. Bhatt, Phys. Rev. Lett. **87**, 107203 (2001).

[19] S.-R. Eric Yang and A.H. MacDonald, Phys. Rev. B **67**, 155202 (2003).

[20] K.M. Yu, W. Walukiewicz, T. Wojtowicz, I. Kuryliszyn, X. Liu, Y. Sasaki, and J.K. Furdyna, Phys. Rev. B **65**, 201303(R) (2002).

[21] J. Schliemann, J. Konig, and A.H. MacDonald, Phys. Rev. B **64**, 165201 (2001).

[22] R.N. Bhatt, Phys. Rev. B **24**, 3630 (1981).

[23] Even if we start with a Heisenberg-like factorization we always find collinear spin ground states.

[24] M.P. Kennett, M. Berciu, and R.N. Bhatt, Phys. Rev. B **66**, 045207 (2002); R.N. Bhatt, X. Wan, M.P. Kennett, and M. Berciu, Comput. Phys. Commun. **147**, 684 (2002).

[25] M.P. Kennett, M. Berciu, and R.N. Bhatt, Phys. Rev. B **65**, 115308 (2002); M. Berciu and R.N. Bhatt, *ibid.* **66**, 085207 (2002).

[26] A. Oiwa, S. Katsumoto, A. Endo, M. Hirasawa, Y. Iye, H. Ohno, F. Matsukura, A. Shen, and Y. Sugawara, Solid State Commun. **103**, 209 (1997).

[27] F. Matsukura, H. Ohno, A. Shen, and Y. Sugawara, Phys. Rev. B **57**, R2037 (1998).

[28] J.G.E. Harris, D.D. Awschalom, F. Matsukura, H. Ohno, K.D. Maranowski, and A.C. Gossard, Appl. Phys. Lett. **75**, 1140 (1999).

[29] Mona Berciu and R.N. Bhatt, Phys. Rev. Lett. **90**, 029702 (2003).

[30] A. Chattopadhyay, S. Das Sarma, and A.J. Millis, Phys. Rev. Lett. **87**, 227202 (2001).

[31] Uniform magnets as well as metallic alloys are characterized by weak deviations from a universal curve on a $M(H,T)/M(00)$ vs T/T_c and $g\mu H/k_B T_c$ plot. [See T. Kaneyoshi, *Introduction to Amorphous Magnets* (World Scientific, Singapore, 1992)], pp. 56–61.

[32] A.L. Chudnovskiy and D. Pfannkuche, Phys. Rev. B **65**, 165216 (2002).

[33] See e.g., S. Oseroff and P.H. Keesom in *Diluted Magnetic Semiconductors*, edited by J.K. Furdyna and J. Kossut (Academic Press, New York, 1988).

[34] G. Zaránd and B. Jankó, Phys. Rev. Lett. **89**, 047201 (2002).

[35] C. Timm, F. Schafer, and F. von Oppen, Phys. Rev. Lett. **90**, 029701 (2003).